Desalination and Water Treatment
www.deswater.com

doi: 10.5004/dwt.2017.0145

58 (2017) 168–180
January

Photocatalytic reduction of Cr (VI) in aqueous solution over ZnO/ HZSM-5 nanocomposite: optimization of ZnO loading and process conditions

Mohsen Haghighi[a], Farhad Rahmani[b], Rouhullah Dehghani[a], Ashraf Mazaheri Tehrani[a], Mohammad Bagher Miranzadeh[a,*]

[a]*Environmental Health Engineering Department, Faculty of Health, Kashan University of Medical Sciences, P.O. Box 8719990000, Kashan, Iran, Tel. +98 9131612852; Fax: +98-31-55540111; email: miranzadehm@ymail.com; web: http://Kaums.ac.ir (M.B. Miranzadeh), Tel. +98 9371993069; email: Mohsenhaghighi087@gmail.com (M. Haghighi), Tel. +98 9133610919; email: dehghani_r@kaums.ac.ir (R. Dehghani), Tel. +98 9364915730; email: mazaheri452@gmail.com (A. Mazaheri)*
[b]*Chemical Engineering Faculty, Sahand University of Technology, P.O. Box 51335-1996, Sahand New Town, Tabriz, Iran, Tel. +98 9359401424; email: Farhad.rahmanichiyane@gmail.com (F. Rahmani)*

Received 1 February 2016; Accepted 14 June 2016

ABSTRACT

The photo-reduction of Cr (VI) was investigated over a series of ZnO-impregnated H-ZSM-5 catalysts varying in ZnO loadings. All the samples were characterized by XRD, FESEM, TEM, EDX, BET, ICP and FT-IR techniques. The XRD analysis confirmed the existence of ZnO and HZSM-5 as crystalline phases in the nanocomposite structure. TEM images illustrated that fine nanoparticles of active metal oxide that were uniformly dispersed over HZSM-5 support. In addition, activity tests were carried out and effects of operational parameters such as initial concentration, reaction time, UV intensity and pH were evaluated. Among the prepared samples, the ZnO/H-ZSM-5 nanocomposite containing 40 wt% ZnO demonstrated the best photocatalytic activity. The full factorial design was applied to optimize the effect of variable factors in the presence of the best photocatalyst. The ANOVA results indicated that at the 95% confidence level, all four variables and their interactions significantly affected the Cr (VI) reduction. In addition, the most effective variable was the initial concentration of Cr (VI). The optimum initial concentration of Cr (VI), pH, UV intensity and reaction time were found to be 10 mg/L, 3, 125 W and 60 min, respectively. Under optimal conditions, complete reduction (>98%) was approximately obtained for Cr (VI).

Keywords: ZnO/HZSM-5; Hexavalent chromium; Photo-reduction; Nanocomposite; Full factorial design

1. Introduction

In recent years, with the development of various industries, the discharge of wastewater containing heavy metals has increased. They cause aquatic environment and soil pollution and their accumulative effects have harmful impacts on human biology [1, 2]. The hexavalent chromium, one of the heavy metals released into aqueous streams, is a direct result of human industrial activities such as electroplating, leather tanning, metal finishing, nuclear power plant, and textile industries [3, 4]. Due to its high toxicity, carcinogenicity, mutagenicity, solubility and significant mobility in environments, it is very dangerous [5–7]. Considering these hazards, Cr (VI) is recognized as a primary pollutant by International Agency for Research on Cancer (IARC). The maximum authorized amount of Cr (VI) in water is limited to 5 mg L^{-1} [8]. Thus, treatment of Cr (VI) to make it less toxic Cr (III) is indispensable. Cr (VI) toxicity has incited researchers to develop new techniques for its removal [4, 9]. In wastewater treatment, various methods have been employed for the removal of Cr

* Corresponding author.

(VI) such as precipitation, electrochemical treatment, ion exchange, reverse osmosis, nanofiltration, bacterial reduction and adsorption [1, 10]. However, such methods are costly and inconvenient and are limited due to high energy requirements with significant sludge production and non-compliance with the standard of water pollution [7, 11]. An alternative clean and convenient method for the removal of Cr (VI) is a photocatalytic process in the presence of a semiconductor such as TiO_2, CdS or WO_3, Fe_2O_3, SnO_2, and so on, under visible or UV radiation [12–14]. Among the semiconductors, nano ZnO performance has been reported to be considerably better than TiO_2, due to its wide band gap 3.37 eV, good optoelectronic, low production cost, thermal stability, its non-toxicity and its low demand for energy in enjoying the ability to operate in the visible light region [15–17]. Despite the positive attributes of ZnO, some of its disadvantages of ZnO such as poor adsorption properties and high recombination rate of the photo-generated e^-/h^+ pairs strongly limit the use of ZnO in environmental remediation [18, 19]. Quick recombination has faster kinetics than surface redox reactions and significantly reduces the efficiency of photocatalysis [20]. To circumvent these limitations, various efforts have been made to improve the efficiency of ZnO via using suitable supports and coupling photocatalysts with other materials such as noble metals [21, 22], semiconductors [23, 24], zeolites [25, 26], and so on. The application of zeolite has been considered as a support, specifically for the application in the field of catalysis due to the thermal stability, uniform pores and channels and excellent adsorption ability [16, 27]. HZSM-5 zeolite with high surface area, surface acidity, ion-exchange capacity, strong adsorption and chemical stable nature is one of the most widely applied materials as catalyst support [28, 29]. It should be mentioned that when a semiconductor oxide is immobilized on the zeolites, it exists as nanosized particle in a highly dispersed form with increased band gap energy and decreased rate of electron–hole recombination [29, 30]. In addition, the excellent adsorption ability of supported semiconductor facilitates the diffusion of pollutant molecule from the solution to the surface of catalysts and thus improves its photocatalytic performance [31]. In addition, the supports with high adsorb-ability can extend life time and reusability of the photocatalyst [32]. Therefore, it seems that ZnO supported on zeolite enhances the photocatalytic activity and induces a synergistic effect [11, 33]. Numerous studies on photo-reduction of Cr (VI) by photocatalyst semiconductors and different adsorbents have been reported during the recent decade. Tabrez A. Khan investigated the removal of Cr(VI) using guar gum-nano ZnO biocomposite [34]. M. Qamar et al. studied the laser-induced efficient reduction of chromium by ZnO nanoparticle [35]. In addition, Wahiba Ketir et al. investigated the characterization and application of $CuCrO_2$/ZnO photocatalysts for the reduction of chromium [36]. In another research, Dadong Shao et al. studied the photocatalytic reduction of Cr (VI) in a solution containing ZnO or ZSM-5 using oxalate as the model organic compound [16]. In spite of numerous species of catalysts for Cr (VI) reduction, there is no report about the photo-reduction of Cr (VI) using ZnO/HZSM-5 nanocomposite. In the present study, the applicability and performance of immobilized ZnO onto HZSM-5 zeolite by impregnation method for photocatalytic reduction of Cr (VI) at different operational conditions was investigated. The influence of different parameters such as ZnO loading amount, initial concentration of Cr (VI), UV light intensity, reaction time and pH on the photo-reduction of Cr (VI) was studied. In addition, factorial design technique was simultaneously used to investigate the effects of interactional parameters on the performance of composite for reduction of Cr (VI). Therefore, optimization of the process parameters affecting the photocatalytic process was performed and a mathematical model was obtained for the process.

2. Materials and methods

2.1. Materials

In the synthesis of ZnO/ZSM-5 nanocomposites, silicic acid, sodium aluminate ($NaAlO_2$, Al_2O_3) and zinc acetate dihydrate ($Zn(O_2CCH_3)_2(H_2O)_2$) were used as silica, alumina and ZnO sources, respectively. In addition, tetra propyl ammonium bromide (TPABr, $C_{12}H_{28}BrN$) was employed as a template. Potassium dichromate ($K_2Cr_2O_7$, 99.9%), acetone and 1, 5-diphenylcarbazide (DFC, 98%) were used in different steps of the experiment. In addition, NaOH and H_2SO_4 were used to adjust the pH value. All of the raw materials were extra pure from Merck and Aldrich Companies. Doubly distilled water was used during the synthesis step and through the experiments.

2.2. Photocatalysts preparation and procedures

The ZnO/HZSM-5 nanocomposites were prepared by impregnation procedure. Zinc acetate dihydrate solution in various concentrations was mixed with the ZSM-5 support, followed by evaporation under constant stirring and then calcination at 300°C for 3 h. The concentration of ($Zn(O_2CCH_3)_2(H_2O)_2$) in solution was matched in order to obtain 10, 20, 30, 40, 50, and 60 wt.% of ZnO content in the final catalysts. The impregnated samples were denoted as ZnO(x)/HZSM-5, where x stands for nominal weight percent of ZnO. The HZSM-5 support was hydrothermally synthesized as mentioned in the literature [37]. First, solutions of Al precursor, Si precursor and TPABr template were prepared. For preparation of Al precursor solution, sodium aluminate was dissolved in NaOH aqueous solution and labelled as solution A. Next, solution B was prepared by dissolving TPABr in NaOH solution and mixing for 30 min and then an aqueous solution of silicic acid was added slowly so that the template and NaOH mixed together. In the next step, solutions A and B were mixed for 60 min to form gel. Then, the solution was poured in a Teflon-lined stainless steel autoclave and heated in a furnace at 180°C for 72 h. After filtration and washing, samples were dried at 110°C for 12 h and then calcined at 550°C for 5 h to form NaZSM-5. Thereafter, the calcined NaZSM-5 powder was turned into the H-form by 2 consecutive ion exchanges with NH_4NO_3 solution (1 M) at 80°C for 12 h followed by filtration and washing. Finally, the obtained sample was dried at 110°C for 12 h and calcinated at 500°C for 5 h. Eventually, H-ZSM-5 was prepared for the synthesis of nanocomposites.

2.3. Photocatalysts characterization methods

X-ray diffraction (XRD) was applied to structural identification that verified the crystallinity of the prepared

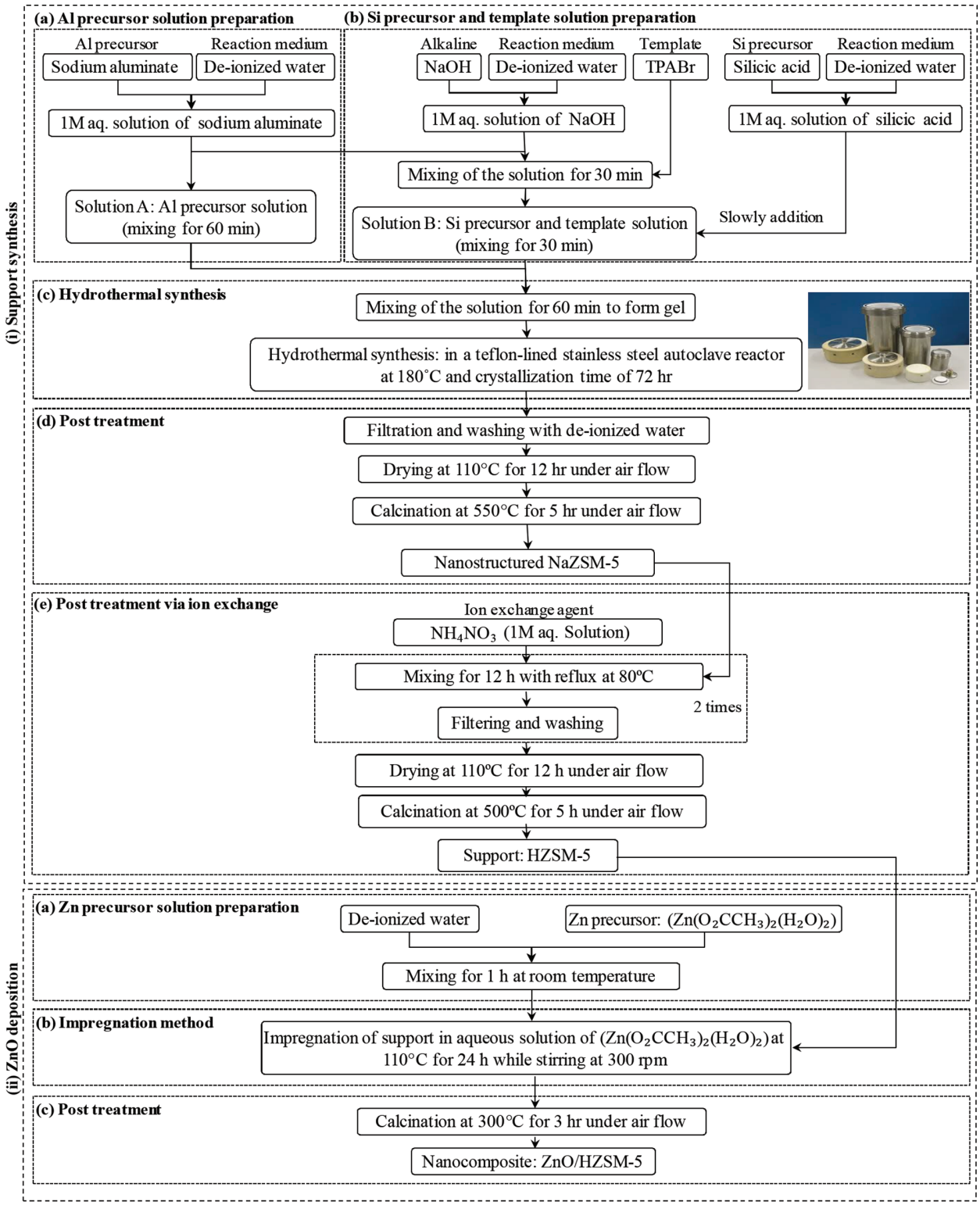

Fig. 1. Synthesis steps of ZnO/HZSM-5 nanocomposite via impregnation/hydrothermal method.

catalysts. It was done via Inel diffractometer EQuniox 3000 in 2–90° 2θ range with mono-chromatized Cu-Ka radiation coupled with X-ray tube operated at 30 mA and 40 kV. The phase identification was made by comparing with the Joint Committee on Powder Diffraction Standards (JCPDSs) database. The morphology and particle size of catalysts were investigated by Field Emission Scanning Electron Microscopy (FESEM) apparatus (HITACHI S-4160). The FT-IR spectrometer (FTIR, BRUKER VECTOR22) was used to investigate the functional groups in the range

of 400–4,000 cm^{-1} wave number. For detecting the metal oxide particles on H-ZSM-5, transmission electron microscopy (TEM) analysis was carried out on a Philips CM-200. The chemical composition of the nanocomposites was measured by energy dispersive X-ray (EDX) analysis integrated into FESEM. Finally, the surface area of the samples was measured by N_2 adsorption using the Quantachrom ChemBET-3000 apparatus.

2.4. Photocatalytic activity analysis

The experimental photo-reactor used for photocatalytic reduction of Cr (VI) has been shown in Fig. 2. Photo-reduction experiments were carried out in a 1 L cylindrical reactor and used a high-pressure mercury lamp (Philips 24 and 125 W) to generate 300–400 nm wave length. The reactor was placed inside a box which was covered by aluminium foil. The reactor temperature was controlled and maintained at 20 ± 1°C by a cooling water flow. The photocatalyst particles were kept suspended in a chromium solution by using a magnetic stirrer. The pH of Cr (VI) solution was adjusted by using NaOH and H_2SO_4 solutions (0.1 M) and was measured by a pH meter. Prior to irradiation, suspensions were magnetically stirred for 30 min in dark conditions to ensure substrate-surface equilibration, and then treated with UV light for different times. After the run, samples were separated from the photocatalyst particles by centrifugation at 4,000 rpm for 5 min. The residual concentration of the Cr (VI) was measured colorimetrically at 540 nm using the 1, 5-diphenylcarbazide (DPC) method. The photocatalytic behaviour of unsupported ZnO was also measured as a reference to that of the ZnO/HZSM-5 composites in the same conditions.

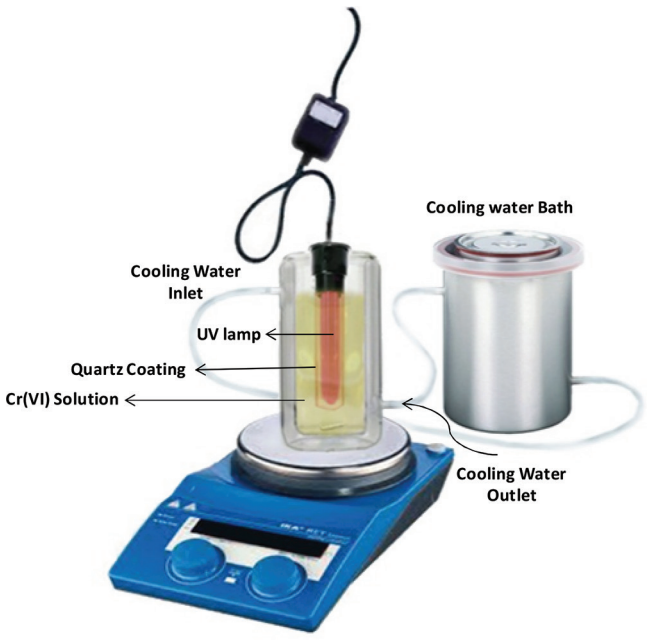

Fig. 2. Experimental set-up for the photocatalytic reduction of hexavalent chromium.

3. Results and discussions

3.1. Photocatalysts characterization

3.1.1. XRD analysis

Fig. 3 depicts the recorded XRD patterns of the synthesized ZnO/HZSM-5 nanocomposite with various loadings of ZnO and Table 1 summarizes the detailed structural and physicochemical properties of these materials. A glance at the XRD patterns reveals that the supported samples show ZnO and HZSM-5 peaks. The diffraction peaks, centred at 2θ = 7.67, 8.61, 14.7, 23.1, 23.35, 23.72 and 23.96 confirmed the presence of HZSM-5 (JCPDS 00-044-0002) in tetragonal phase.

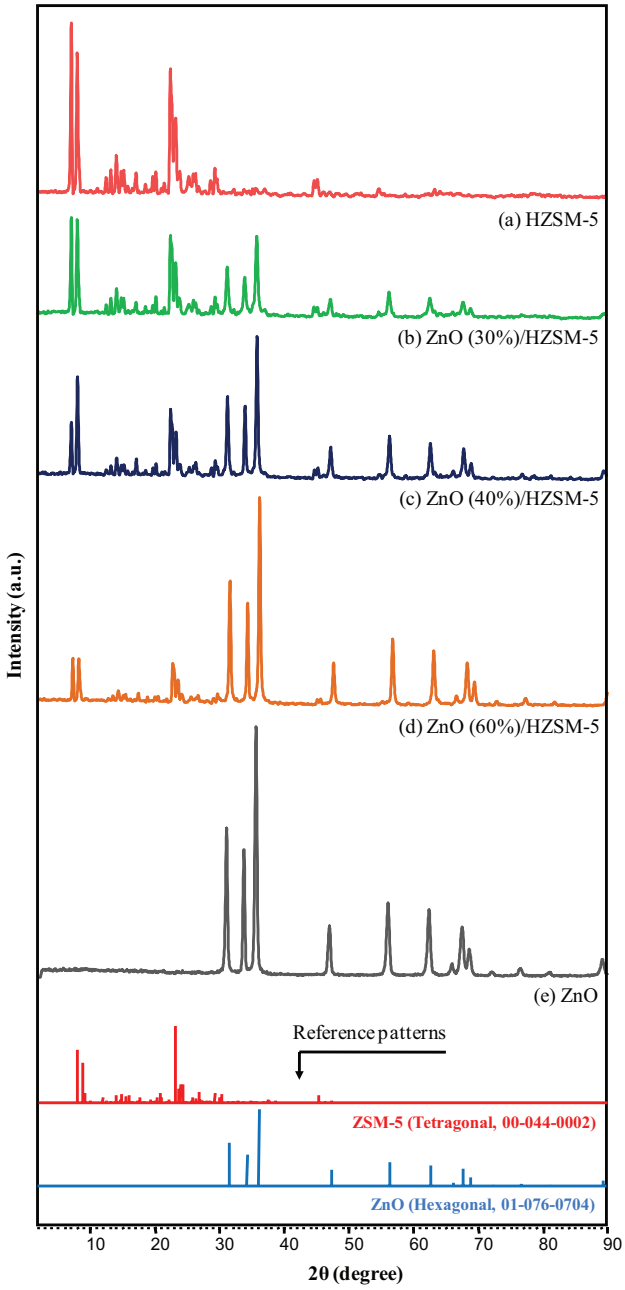

Fig. 3. XRD patterns of synthesized ZnO/HZSM-5 nanocomposite with various ZnO loading.

Table 1
BET specific surface area and ICP analysis of synthesized ZnO/HZSM-5 nanocomposite via various ZnO loading

Samples	Synthesis method	ZnO (wt.%)	Zn content (wt.%)		S_{BET} (m^2/g)	Relative crystallinity (%)	
			ICP	EDX		ZnO[a]	HZSM-5[b]
HZSM-5	Hydrothermal	0	0	0	372	–	100
ZnO (30%)/HZSM-5	Hydrothermal/impregnation	30	25.12	22.95	325.2	32.093	57.70
ZnO (40%)/HZSM-5	Hydrothermal/impregnation	40	31.2	29.23	295	57.66	45.65
ZnO (60%)/HZSM-5	Hydrothermal/impregnation	60	50.53	47.31	218	85.926	26.454
ZnO	Impregnation	100	84.6	80.82	16	100	–

[a]Defined as relative intensity of XRD patterns at 2θ = 31.89, 34.55 and 36.39° based on the highly crystalline ZnO sample.
[b]Defined as relative intensity of XRD patterns at 2θ = 7.67, 796.67 and 233.102° based on the highly crystalline HZSM-5 sample.

In addition, the appeared peaks at 2θ = 31.89, 34.55, 36.39, 47.69, 56.77, 63.03 and 68.22 are assigned to ZnO (JCPDS 01-076-0704) in hexagonal phase. With comparison of XRD patterns, it is observed that by gradually increasing the ZnO content over HZSM-5 structure, the peaks related to ZnO appear and obviously become sharper. In contrast, the intensity of ZSM-5 peaks in the synthesized samples decreases. As shown in Table 1, the relative crystallinity of ZnO increases by increasing the ZnO content.

3.1.2. FESEM analysis

FESEM images of synthesized samples with different ZnO loadings are presented in Fig. 4. As it can be seen, HZSM-5 sample has a coffin-shaped structure, in agreement with that of HZSM-5 reported in the literature [38, 39]. By ZnO loading, tiny worm like particles were formed over the HZSM-5 structure. By further increasing the metal oxide content, the surface was covered with a greater amount of small nano-scale ZnO particles and thereupon, the presence of HZSM-5 particles was hardly distinguished. This reflects that relatively more HZSM-5 coverage, as a result of ZnO loading, decreases the relative crystallinity for HZSM-5 phase compared with other ones which is in accordance with XRD results. Accordingly, it seems that the surface particles observed in the FESEM images of nanocomposites are mainly attributed to ZnO particles. A close examination of the FESEM results also revealed that the samples lean in ZnO content showed relatively open morphology and low numbers of agglomerations. It can be observed from these images that the synthesized catalysts have nanometric surface particles. Nanoparticles provide more reactive and reducible sites and result in a high catalytic performance of the composite. Compared with pure ZnO particles, supported ZnO samples exhibit smaller particles. Increasing metal oxide content would result in higher numbers of active sites for the photocatalytic process. Nonetheless, irregular agglomerations and considerable blocking of the support's pores can be consider as the disadvantageous side effects of excessive loading of active component and may lead to worse catalytic performance. Therefore, it can be minimized by employing a proper ZnO loading.

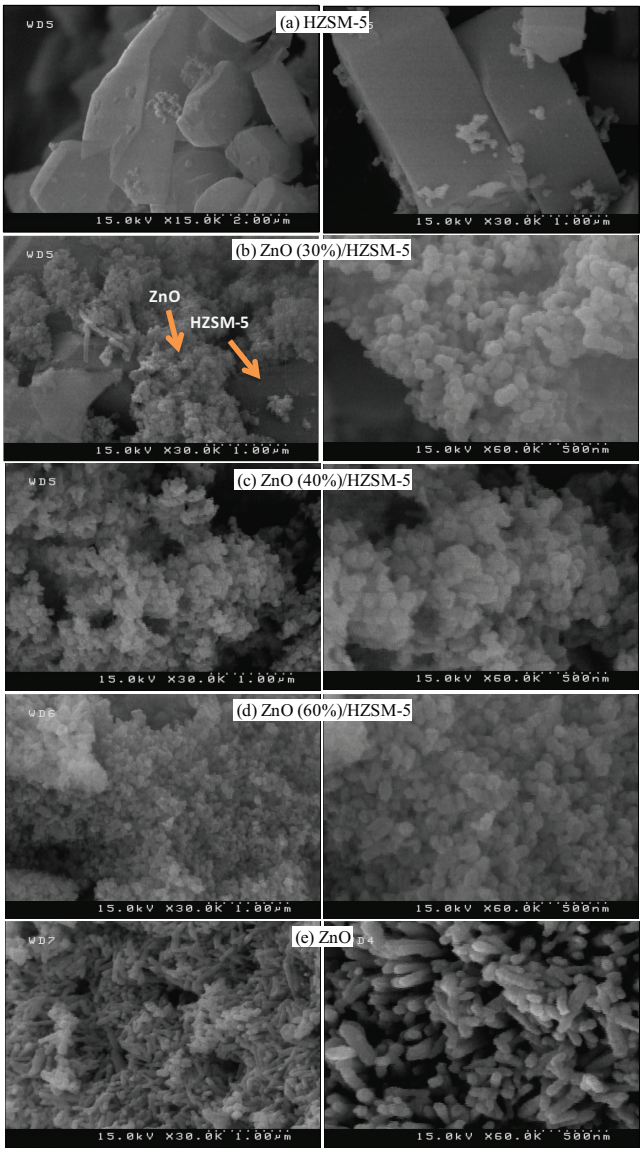

Fig. 4. FESEM images of synthesized ZnO/HZSM-5 nanocomposite with various ZnO loading.

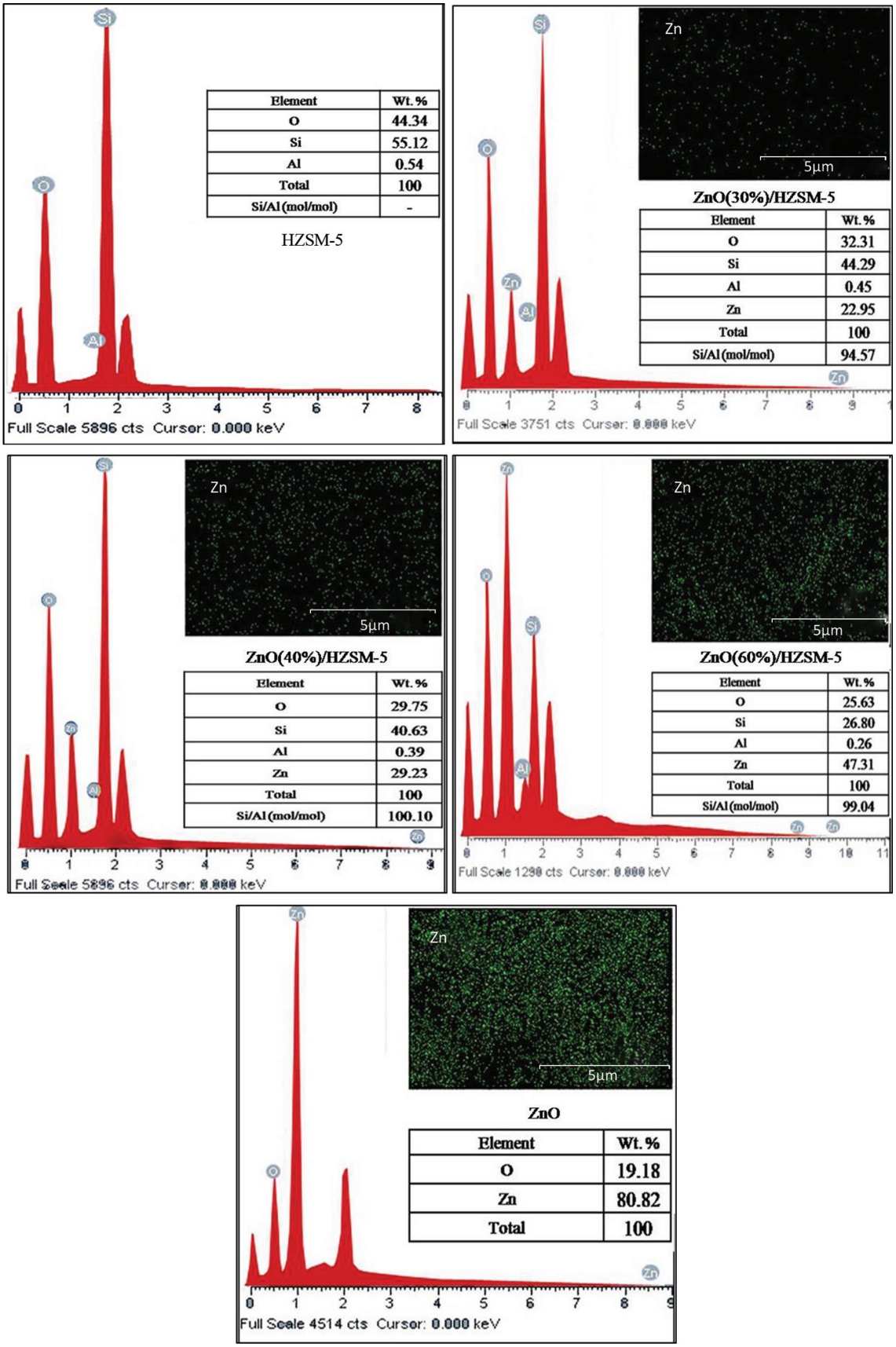

Fig. 5. EDX analysis of synthesized ZnO/HZSM-5 nanocomposite via various ZnO loading.

3.1.3. EDX analysis

It is well known that the dispersion of supported zinc species is a major factor affecting the intrinsic activity of Zn containing photocatalysts. To determine the elemental composition, ensure the synthesis procedure and also assess the dispersion of Zn species in the synthesized samples, the EDX analysis was carried out. The EDX micrographs, including spectrums and Zn dot-mappings, were shown in Fig. 6. The EDX spectra demonstrate the existence of only Al, O, Si and Zn elements, confirming the absence of any impurities in the sample structure. Interestingly, the Zn content and Si/Al ratio of the synthesized samples obtained by the EDX spectra and the corresponding initial gel, given in Table 1, are close to each other. This is an additional evidence for the successful synthesis and more importantly, the ability of HZSM-5 support to uniformly disperse Zn species. Generally, the EDX dot-mapping results depicted that apt dispersion of Zn was attained for all supported samples as expected. A close examination of the EDX dot-mapping results reveals that the optimum percentage of loading for better dispersion of Zn is 40%. In other words, increasing Zn content from 40% to 60% has decreased the dispersion of active metal oxide, which could be addressed by the appearance of agglomerations. That is to say, EDX of the investigated samples confirms that the catalytic process is affected by much higher dispersion of active component for ZnO (40%)/HZSM-5 compared with other ones.

3.1.4. TEM analysis

To have an insight into the nature and dimensions of the supported ZnO species, TEM analysis of the ZnO/HZSM-5 nanocomposite with 40% loading of ZnO was carried out and illustrated in Fig. 8. The black dots on the bright background are particles of the metals oxide on the surface of the supports. Finely dispersed small ZnO species in the nanoscale on the external surface of zeolite crystals are the evidence for the ZnO(40%)/HZSM-5 composite. As it is observed, all the metal oxide particles less than 40 nm and Zn species over HZSM-5 are homogeneous and highly dispersed. This result is in close agreement with EDX analysis. In addition, a superior interaction between the support and the metal oxide particles can be concluded from the TEM micrographs which are responsible for controlling the size of Zn ensembles.

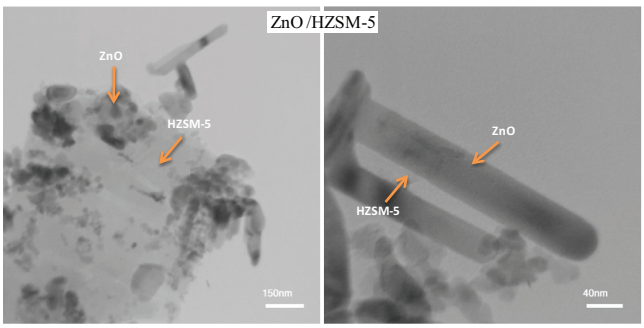

Fig. 6. TEM images of synthesized ZnO/HZSM-5 nanocomposite containing 40 wt% ZnO.

3.1.5. BET analysis

One of the most influential parameters of the heterogeneous photocatalysts is their specific surface area. Higher surface area facilitates the reactants adsorption and provides more active sites which are responsible for improving the photocatalytic performance. The BET surface area (S_{BET}) of synthesized samples is listed in Table 1. Reported results in the literature show the surface area in the range of 300–400 m^2/g and 5–40 m^2/g for HZSM-5 and ZnO, respectively [40, 41]. As it can be seen, bare HZSM-5 and pure ZnO exhibited a surface area of 372 and 16 m^2/g, respectively. The examination of obtained results reveals that upon addition of ZnO to bare HZSM-5, the surface area decreased depending on the ZnO loading. All ZnO containing samples have a smaller surface area in comparison with the bare support. This behaviour can be attributed to the deposition of zinc species into micro pores which partially blocks them. The loss of HZSM-5 crystallinity also supports this hypothesis. The surface area of ZnO-loading samples decreased gradually with increasing ZnO content up to 40%. However, the surface loss significantly occurred with further increase of the ZnO content. This can be justified by greater metal oxide loading and the appearance of agglomerations which is in accordance with FESEM images.

3.1.6. FTIR analysis

Fig. 7 indicates the FTIR spectrums of ZnO/HZSM-5 samples synthesized by various ZnO loading in a wide range of frequency 400–4,000 cm^{-1}. This observation reveals that the FTIR patterns of synthesized composite have a similar trend in all contents of ZnO loadings and a significant change is not observed. The broad peaks at 3,616 and 1,551 cm^{-1} are attributed to interacting OH or to bridging OH groups [42, 43]. The other recorded peak at 1,551 cm^{-1} can be ascribed to physically absorbed water which means the nanocomposites adsorbed water in air [44, 45]. In addition, recorded peaks in the FTIR spectrum of HZSM-5 in the range of 400–1,200 cm^{-1} wave number could be related to Si-O(Si) and Si-O(Al) vibration in tetrahedral or alumina- and silico-oxygen bridges [46]. Meanwhile, the peak in the range of 400–500 cm^{-1} can correspond to the stretching vibration of ZnO which might be overlapped with T-O stretching frequency (considered insensitive to zeolite structure) and therefore the overlap peak can be seen in this region [47]. It is worth mentioning that the zeolite structure does not change when a transition metal oxide cation enters into a zeolite structure and just some slight shifts occur at the peaks which can be seen by comparing spectrums [48]. These results confirm the sufficient loading of ZnO over HZSM-5 zeolite.

3.2. Photocatalytic performance of ZnO/HZSM-5 toward reduction of Cr (VI)

3.2.1. Effect of ZnO loading on photocatalytic performance

The photo-reduction efficiencies of Cr (VI) by ZnO/HZSM-5 composite containing different ZnO loadings under UV light irradiation are shown in Fig. 8. At the beginning of the UV irradiation, adsorption saturation was almost achieved, and thus the adsorption had little contribution

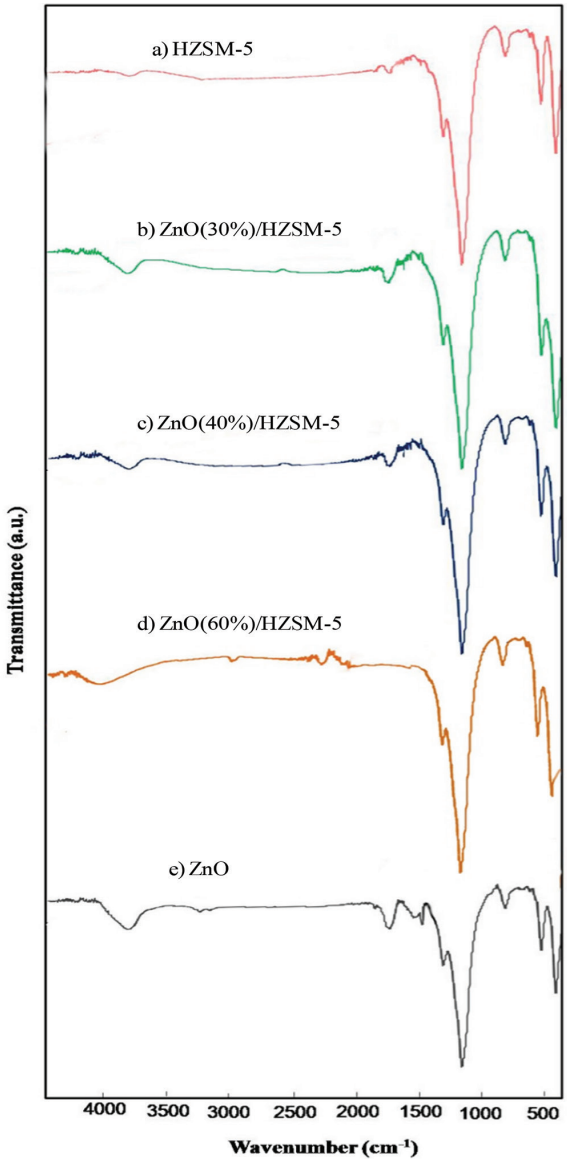

Fig. 7. FTIR spectra of synthesized ZnO/HZSM-5 nanocomposite via various ZnO loading.

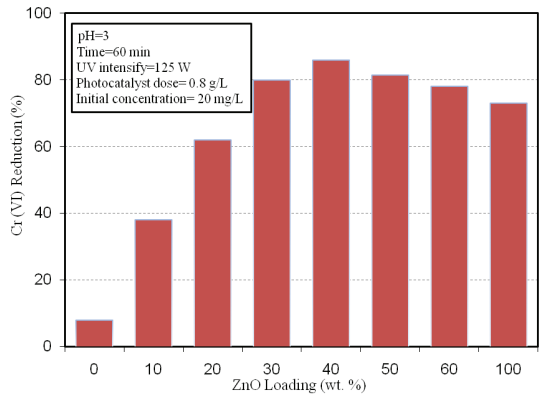

Fig. 8. Effect of different ZnO loading on photocatalytic performance.

during the photo-degradation. The variation of ZnO content obviously indicates that 40 wt.% is the optimum content of ZnO in ZnO/HZSM-5 nanocomposites for the best photocatalytic performance. This could be expected according to characterization results. The excessive loadings of ZnO alleviate the results in the significant decrease of surface area, appearance of more number of agglomerations and surface coverage of HZSM-5 which alleviate the synergetic effect of ZnO. After 60 min of UV light irradiation, 87% of the initial Cr (IV) was photo-degraded by ZnO (40%)/HZSM-5 nanocomposite, whereas 72% of the initial Cr (IV) was decomposed by unsupported ZnO. This superior performance is attributed to the higher surface area, better dispersion and smaller size of ZnO particles, less number of surface agglomerations and also high adsorption ability of HZSM-5.

3.2.2. Statistical study

The full factorial design was used to optimize and create the relationship between the responses (reduction of Cr (VI)) and the factors including UV light intensity (factor A), reaction time (factor B), pH (factor C) and Cr (VI) initial concentration (factor D). Analysis of variance (ANOVA) was investigated to further specify the most significant interaction effects of factors on the reduction of Cr (VI). The ANOVA analysis indicates the findings on the significance of the main interaction effects with a confidence level of 95% (Table 2). Based on the ANOVA results, all of the main factors (A, B, C and D) were found to have significant effects on the reduction of Cr (VI). Considering the F-values that determine the order of the major factor effect, it can be seen that the main factors have positive effects on the Cr (VI) reduction. Meanwhile, the initial concentration of Cr (VI) is the most important parameter (F-value = 655.70) compared with other main factors and interactions on the response. Ironically, the two main factors of pH and reaction time indicated a significant interaction ($p < 0.05$) with F_0 value 41.73. This means that the effect of reaction time on reduction of Cr (VI) depends on the levels of pH values. In addition, ANOVA results indicate the statistically significant effect of main factors and some of the interactions with p-value less than 0.05. Finally, the proportional model of Cr (VI) reduction was calculated by the coefficient of determination R^2 (Table 2). The high value of F_0 (94.9283) also confirms the significance of the proposed model.

3.3. Contribution of each parameter on reduction of Cr (VI)

3.3.1. Effect of pH on Cr (VI) photo-reduction efficiency

In the photocatalytic process, increasing pH value enhances the conversion of $Cr_2O_7^{2-}$ to CrO_4^{2-} as predominant species, resulting in lower reduction of Cr (VI). The pH_{ZPC} (zero-point charge pH) of ZnO is 8.3. In pH_{ZPC}, the catalyst surface by positive and negative charges is equally affected. It seems that a layer of ZnO particles has formed around the HZSM-5 and hence pH_{ZPC} of the composite is about 8.3. Therefore, with decreasing pH to less than pH_{ZPC}, the catalyst surface is charged positively (due to specific adsorption of H^+ ions) and facilitates the reduction process. On the other hand, when the pH > pH_{ZPC}, the surface

Table 2
Analysis of variance for Cr (VI) photo-reduction efficiency

Source	Degrees of freedom	Sum of squares	Mean square	F_0	P-value
A	1	1,996.91	1,996.91	273.92	0.000
B	2	7,505.90	3,752.95	514.79	0.000
C	2	7,638.53	3,819.27	523.89	0.000
D	3	14,340.66	4,780.22	655.70	0.000
A.B	2	203.94	101.97	13.99	0.001
A.C	2	203.63	101.82	13.97	0.001
A.D	3	156.65	52.22	7.16	0.005
B.C	4	1,216.87	304.22	41.73	0.000
B.D	6	412.13	68.69	9.42	0.001
C.D	6	467.35	77.89	10.68	0.000
A.B.C	4	116.44	29.11	3.99	0.028
A.B.D	6	13.77	2.30	0.31	0.0917
A.C.D	6	11.29	21.88	3.00	0.050
B.C.D	12	78.29	6.52	0.89	0.575
Error	12	87.48	7.29		
Total	71	34,569.85			
Standard deviation 2.7004		R^2 99.75%		R^2 (adjusted) 98.50%	

Proposed model information for Cr (VI) reduction efficiency and analysis of variance for testing its significance

(A) The proposed model information

Cr (VI) reduction (%) = 31.2886 + 0.15438A + 1.35117B – 1.68329C – 0.829621D + 0.00417853AB – 0.013717AC – 0.00471543AD – 0.115274BC – 0.0119687BD + 0.0588034CD – 0.000437809ABC + 0.000454373ACD
Standard deviation = 5.37149, R^2 = 95.08%, R^2 (adjusted) = 94.07%

(B) The analysis of variance for proposed model

Source	Degrees of freedom	Sum of squares	Mean square	F_0	P-value
Regression	12	32,867.5	2,738.96	94.9283	0.000
Error	59	1702.3	28.85		
Total	71	34,569.8			

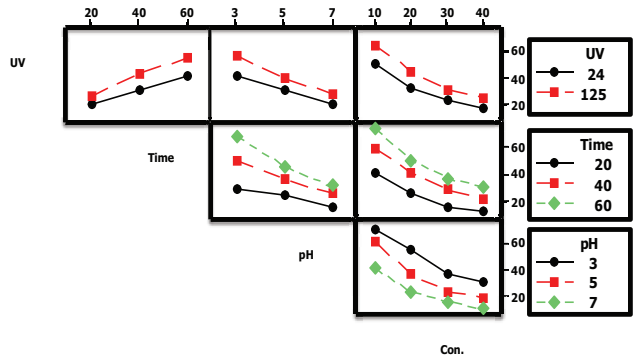

Fig. 9. Effect of different parameter on photocatalytic performance.

of the catalyst is negatively charged. Hence, the reduction efficiency decreases [9, 11, 49]. Fig. 9 illustrates the influence of pH value on the Cr (VI) photo-reduction process. The change in pH has an important effect on the Cr (VI) reduction and its residual concentration as decreasing pH will increase the removal rates of Cr (VI). Similar observations were reported before by Jing and Dipti [5, 50]. As shown in Fig. 9, the removal of Cr (VI) was ~100% at pH ≤ 3. Then, the removal of Cr (VI) decreased slowly to ~90% as pH value increased to 5 and then only ~60% Cr (VI) was removed when the pH value increased to ~7. Generally, the removal of chromium with changes in pH value occurs following these reactions [51]:

(1) At acidic conditions

$$Cr_2O_7^{-2} + 14H^+ + 6e^- \rightarrow 2Cr(III) + 7H_2O \quad (1)$$

(2) At Neutrals conditions

$$Cr_2O_4^{(-2)} + 8H^+ + 3e^- \rightarrow Cr(III) + 4H_2O \quad (2)$$

(3) At Alkaline conditions

$$Cr_2O_4^{-2} + 4H_2O + 3e^- \rightarrow Cr(OH)_3 + 5OH^- \quad (3)$$

3.3.2. Photocatalytic reduction of Cr (VI) at different Cr (VI) initial concentrations

Photocatalytic reduction of Cr (VI) at T = 20 ± 1°C at different Cr (VI) initial concentrations is shown in Fig. 9. As it can be seen, the Cr (VI) removal efficiency strongly depends on initial chromium concentration. With increasing the Cr (VI) concentration, the reduction rate of chromium gradually decreases. With a fixed ZnO/HZSM-5 dose, the increased chromium concentration results in more adsorption of Cr (VI) ions to ZnO/HZSM-5 composite which can cause the total available adsorption sites to be restricted [9, 52, 53]. Moreover, increasing concentration of the chromium has an inhibitor role to reach UV irradiation to the catalyst surface [12]. This claim has been confirmed by Young and Quanping [54, 55]. As shown in Fig. 9, the photocatalytic reduction of Cr (VI) was decreased from ~100% to nearly 57.7% with increasing the initial Cr (VI) concentration from 10 to 40 mg/L after 60 min.

3.3.3. Effect of illumination time and UV light intensity

Fig. 9 displays the Cr (VI) reduction by ZnO/HZSM-5 nanocomposite when intensity of UV illumination is varied from 24 to 125 W. It can be seen that with increasing the UV light intensity and illumination time, the reduction rate of Cr (VI) increases. This event has been reported by Te Hsu and Shing previously. It is attributed to more electron-hole pairs which are produced under higher illumination intensity. Hence, more electrons will be available for reduction of chromium [56–58]. The reduction rate of Cr (VI) was ~100% within 60 min under the illumination intensity of 125 W which decreased to ~84% with decreasing UV intensity to 24 W. On the other hand, the reduction rate of chromium increased quickly from ~54% to nearly 100% with increasing the illumination time.

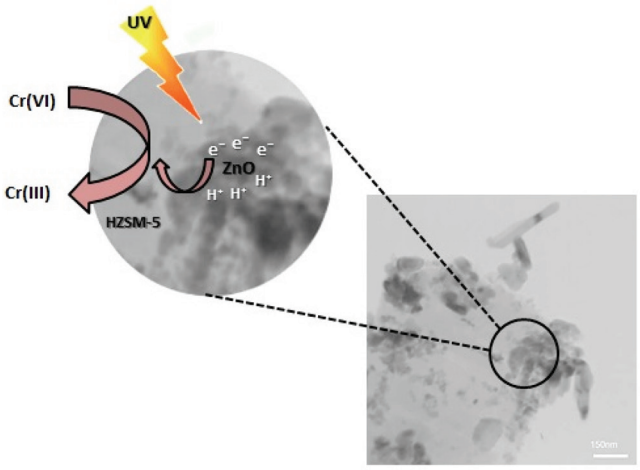

Fig. 10. Schematic diagram of ZnO/HZSM-5 nanocomposite mechanism under UV light for photocatalytic reduction of Cr (VI).

3.4. Photocatalytic performance comparison of different catalysts evaluated for the Cr (VI) photo-reduction

To evaluate better, the synthesized composite better and ensure its performance, the photocatalytic activity was compared with those reported in the literature. Table 3 indicates the different composites evaluated in the Cr (VI) photo-reduction in aqueous solution. The percentage of Cr (VI) reduction is a suitable criterion to compare the obtained results in cited literature in order to ascertain the synergetic effect of employing composite. According to the activity information and conditions of experiments, which were listed in Table 3, ZnO/H-ZSM-5 composite seems to have the appropriate performance towards Cr (VI) photo-reduction. In addition, considerable activity was found over TiO_2/Chitosan, ZnO/Kaoline, Fe_2O_3/clay and ZnO/Graphene composites. However, the reaction time and light intensity of the two latter composites are greater and it can improve the efficiency of the process. In addition, despite having better operational conditions, the TiO_2/diatomite composite had lower efficiency.

3.5. Plausible reaction pathway of Cr (VI) photo-reduction over ZnO/HZSM-5

The photo-reduction of Cr (VI) occurs following two main steps: First, Cr (VI) is adsorbed on H-ZSM-5 and the reaction occurs slightly on its surface. Then, Cr (VI) and its intermediates transfer to the ZnO surface to carry on photocatalytic reaction. According to the mentioned steps, various factors can be important in photo-reduction of Cr(VI) by ZnO/H-ZSM-5 nanocomposite: (a) The large specific area of adsorbent which adsorbs Cr (VI) molecules and

Table 3
Photocatalytic performance of different catalysts for the photo-reduction of Cr (VI)

Composite	Concentration	Time (min)	Light intensity (W)	pH	Dose	Removal (%)	Reference
ZnO/HZSM-5	10 mg/L	60	125	3	0.8 g/L	98.2	Present work
ZnO/Graphene	10 mg/L	240	500	–	1 g/L	96	[61]
ZnO/Kaoline	30 mg/L	120	125	4	1 g/L	88.3	[64]
ZnO/CuO	–	60	20	4.6	–	55	[65]
Fe_2O_3/Clay	50 ppm	300	200	2	1 mg/ml	95	[11]
TiO_2/Chitosan	50 mg/L	60	32	2	100 mg	91.4	[62]
ZnO	15 mg/L	120	125	7	1 g/L	78	[66]
S-ZVIN	100 mg/L	90	-	3	–	88.44	[67]
TiO_2/diatomite	10 mg/L	180	300	2.1	2 g/L	57.83	[56]

creates active sites for photocatalytic reaction; (b) quick transfer of adsorbed molecules from H-ZSM-5 to ZnO, which this process accelerates with increasing the surface of adsorbent; and (c) the performance of ZnO in photocatalytic reaction [59, 60]. On the other hand, the high performance of the ZnO/H-ZSM-5 composite in photo-reduction of Cr (VI) can be attributed to the coordination between H-ZSM-5 and ZnO that H-ZSM-5 has large specific area and ZnO, due to its position of valence band, has strong photo-generated holes [15, 59]. In addition, the surface modification of ZnO using H-ZSM-5 leads to high electron mobility and suppresses the electron-hole recombination which causes a decrease in the photo-reduction of Cr (VI) [61]. The followings are the suggested reactions responsible for the photo-reduction of Cr (VI) using ZnO/H-ZSM-5 composite.

During the photocatalytic process, ZnO semiconductor adsorbs photon and promotes of an electron from the valance band to the conduction band and produces an electron-hole pair (Eq. (4)). Recombination of photo-generated electrons and hole may occur (Eq. (5)). Photoelectrons transfer to H-ZSM-5 and electron-holes pairs are separated (Eq. (6)). Photoelectrons can reduce Cr (VI) to Cr (III) (Eq. (7)) [26, 62, 63].

$$ZnO + h\upsilon \rightarrow ZnO(h^{+}_{VB} + e^{-}_{CB}) \quad (4)$$

$$e^{-} + h^{+} \rightarrow \text{heat} \quad (5)$$

$$ZnO\left(h^{+}_{VB} + e^{-}_{CB}\right) + HZSM-5 \rightarrow ZnO\left(h^{+}_{VB}\right) + HZSM-5(e^{-}_{CB}) \quad (6)$$

$$Cr_2O_7^{2-} + 14H^{+} + 6e^{-} \rightarrow 2Cr^{3+} + 7H_2O \quad (7)$$

4. Conclusions

In this study, a series of ZnO/H-ZSM-5 nanocomposite with different contents of ZnO loading were successfully synthesized via impregnation method for photo-reduction of Cr (VI). The EDX and XRD results confirmed the correct formation of ZnO/H-ZSM-5 composite. TEM analysis indicates dispersion of nanoscale ZnO on the external surface of zeolite. Moreover, activity tests illustrated that the sample with the 40% ZnO loading had the best performance in photo-reduction of Cr (VI). Most of all, the excellent performance of composite in reduction of Cr (VI) could be attributed to (a) huge specific surface area of H-ZSM-5, (b) synergic effect between ZnO and H-ZSM-5 and (c) effective separation of electron-hole pairs and reduction of their recombination rate. Finally, the results approve that ZnO/H-ZSM-5 with ~98.2% reduction of Cr (VI) in optimum conditions is an efficient and proper catalyst for controlling Cr (VI) pollution in water and wastewater.

Acknowledgements

The authors gratefully acknowledge Kashan University of Medical Science for the financial support of the project as well as Iran Nanotechnology Initiative Council for complementary financial support.

References

[1] K.Z. Setshedi, M. Bhaumik, M.S. Onyango, A. Maity, High-performance towards Cr (VI) removal using multi-active sites of polypyrrole–graphene oxide nanocomposites: batch and column studies, Chem. Eng. J., 262 (2015) 921–931.
[2] H. Wang, X. Yuan, Y. Wu, X. Chen, L. Leng, H. Wang, H. Li, G. Zeng, Facile synthesis of polypyrrole decorated reduced graphene oxide–Fe3O4 magnetic composites and its application for the Cr (VI) removal, Chem. Eng. J., 262 (2015) 597–606.
[3] H. Figueiredo, C. Quintelas, Tailored zeolites for the removal of metal oxyanions: overcoming intrinsic limitations of zeolites, J. Hazard. Mater., 274 (2014) 287–299.
[4] R. Khosravi, M. Fazlzadehdavil, B. Barikbin, A.A. Taghizadeh, Removal of hexavalent chromium from aqueous solution by granular and powdered Peganum Harmala, Appl. Surf. Sci., 292 (2014) 670–677.
[5] J. Guo, Y. Li, R. Dai, Y. Lan, Rapid reduction of Cr (VI) coupling with efficient removal of total chromium in the coexistence of Zn (0) and silica gel, J. Hazard. Mater., 243 (2012) 265–271.
[6] S. Xu, Y. Zhang, S. Pan, H. Ding, G. Li, Recyclable magnetic photocatalysts of Fe 2+/TiO2 hierarchical architecture with effective removal of Cr (VI) under UV light from water, J. Hazard. Mater., 196 (2011) 29–35.
[7] G. Zelmanov, R. Semiat, Iron (Fe+3) oxide/hydroxide nanoparticles-based agglomerates suspension as adsorbent for chromium (Cr+6) removal from water and recovery, Sep. Purif. Technol., 80 (2011) 330–337.
[8] M. Kebir, M. Chabani, N. Nasrallah, A. Bensmaili, M. Trari, Coupling adsorption with photocatalysis process for the Cr (VI) removal, Desalination, 270 (2011) 166–173.
[9] M. Naimi-Joubani, M. Shirzad-Siboni, J.-K. Yang, M. Gholami, M. Farzadkia, Photocatalytic reduction of hexavalent chromium with illuminated ZnO/TiO2 composite, J. Ind. Eng. Chem., 22 (2015) 317–323.
[10] M. Sabonian, M.A. Behnajady, Artificial neural network modeling of Cr (VI) photocatalytic reduction with TiO2-P25 nanoparticles using the results obtained from response surface methodology optimization, Desalin. Water Treat., 56 (2015) 2906–2916.
[11] H. Mekatel, S. Amokrane, B. Bellal, M. Trari, D. Nibou, Photocatalytic reduction of Cr (VI) on nanosized Fe2O3 supported on natural Algerian clay: characteristics, kinetic and thermodynamic study, Chem. Eng. J., 200 (2012) 611–618.
[12] S. Chakrabarti, B. Chaudhuri, S. Bhattacharjee, A.K. Ray, B.K. Dutta, Photo-reduction of hexavalent chromium in aqueous solution in the presence of zinc oxide as semiconductor catalyst, Chem. Eng. J., 153 (2009) 86–93.
[13] S. Tuprakay, W. Liengcharernsit, Lifetime and regeneration of immobilized titania for photocatalytic removal of aqueous hexavalent chromium, J. Hazard. Mater., 124 (2005) 53–58.
[14] H. Eskandarloo, A. Badiei, M.A. Behnajady, G.M. Ziarani, Minimization of electrical energy consumption in the photocatalytic reduction of Cr (VI) by using immobilized Mg, Ag co-impregnated TiO2 nanoparticles, RSC Adv., 4 (2014) 28587–28596.
[15] A. Di Paola, E. García-López, G. Marcì, L. Palmisano, A survey of photocatalytic materials for environmental remediation, J. Hazard. Mater., 211 (2012) 3–29.
[16] D. Shao, X. Wang, Q. Fan, Photocatalytic reduction of Cr (VI) to Cr (III) in solution containing ZnO or ZSM-5 zeolite using oxalate as model organic compound in environment, Microporous Mesoporous Mater., 117 (2009) 243–248.
[17] B. İkizler, S.M. Peker, Synthesis of TiO2 coated ZnO nanorod arrays and their stability in photocatalytic flow reactors, Thin Solid Films, (2015).
[18] C. Yu, K. Yang, Y. Xie, Q. Fan, C.Y. Jimmy, Q. Shu, C. Wang, Novel hollow Pt-ZnO nanocomposite microspheres with hierarchical structure and enhanced photocatalytic activity and stability, Nanoscale., 5 (2013) 2142–2151.
[19] S. Anandan, A. Vinu, N. Venkatachalam, B. Arabindoo, V. Murugesan, Photocatalytic activity of ZnO impregnated Hβ and mechanical mix of ZnO/Hβ in the degradation of monocrotophos in aqueous solution, J. Mol. Catal. A: Chem., 256 (2006) 312–320.

[20] R. Cai, J.-g. Wu, L. Sun, Y.-j. Liu, T. Fang, S. Zhu, S.-y. Li, Y. Wang, L.-f. Guo, C.-e. Zhao, 3D graphene/ZnO composite with enhanced photocatalytic activity, Mater. Des., 90 (2016) 839–844.
[21] T. Hirakawa, P.V. Kamat, Charge separation and catalytic activity of Ag@ TiO2 core-shell composite clusters under UV-irradiation, J. Am. Chem. Soc., 127 (2005) 3928–3934.
[22] P. Li, Z. Wei, T. Wu, Q. Peng, Y. Li, Au–ZnO hybrid nanopyramids and their photocatalytic properties, J. Am. Chem. Soc., 133 (2011) 5660–5663.
[23] S. Elder, F. Cot, Y. Su, S. Heald, A. Tyryshkin, M. Bowman, Y. Gao, et al., The discovery and study of nanocrystalline TiO2-(MoO3) core-shell materials, J. Am. Chem. Soc., 122 (2000) 5138–5146.
[24] J. Yang, J. Dai, J. Li, Visible-light-induced photocatalytic reduction of Cr (VI) with coupled Bi2O3/TiO2 photocatalyst and the synergistic bisphenol A oxidation, Environ. Sci. Pollut. Res., 20 (2013) 2435–2447.
[25] J. Chen, Z. Feng, P. Ying, C. Li, ZnO clusters encapsulated inside micropores of zeolites studied by UV Raman and laser-induced luminescence spectroscopies, J. Phys. Chem. B, 108 (2004) 12669–12676.
[26] A. Nezamzadeh-Ejhieh, S. Khorsandi, Photocatalytic degradation of 4-nitrophenol with ZnO supported nano-clinoptilolite zeolite, J. Ind. Eng. Chem., 20 (2014) 937–946.
[27] M. Khatamian, Z. Alaji, Efficient adsorption-photodegradation of 4-nitrophenol in aqueous solution by using ZnO/HZSM-5 nanocomposites, Desalination, 286 (2012) 248–253.
[28] W. Zhang, K. Wang, Y. Yu, H. He, TiO2/HZSM-5 nano-composite photocatalyst: HCl treatment of NaZSM-5 promotes photocatalytic degradation of methyl orange, Chem. Eng. J., 163 (2010) 62–67.
[29] M. Takeuchi, T. Kimura, M. Hidaka, D. Rakhmawaty, M. Anpo, Photocatalytic oxidation of acetaldehyde with oxygen on TiO2/ZSM-5 photocatalysts: effect of hydrophobicity of zeolites, J. Catal., 246 (2007) 235–240.
[30] M. Noorjahan, V.D. Kumari, M. Subrahmanyam, P. Boule, A novel and efficient photocatalyst: TiO2-HZSM-5 combinate thin film, Appl. Catal. B, 47 (2004) 209–213.
[31] Y. Gao, X. Pu, D. Zhang, G. Ding, X. Shao, J. Ma, Combustion synthesis of graphene oxide–TiO2 hybrid materials for photodegradation of methyl orange, Carbon., 50 (2012) 4093–4101.
[32] M. Bahrami, A. Nezamzadeh-Ejhieh, Effect of the supported ZnO on clinoptilolite nano-particles in the photodecolorization of semi-real sample bromothymol blue aqueous solution, Mater. Sci. Semicond. Process., 30 (2015) 275–284.
[33] C. Wang, H. Shi, Y. Li, Synthesis and characteristics of natural zeolite supported Fe3+-TiO2 photocatalysts, Appl. Surf. Sci., 257 (2011) 6873–6877.
[34] T.A. Khan, M. Nazir, I. Ali, A. Kumar, Removal of chromium (VI) from aqueous solution using guar gum–nano zinc oxide biocomposite adsorbent, Arabian J. Chem., (2013).
[35] M. Qamar, M. Gondal, Z. Yamani, Laser-induced efficient reduction of Cr (VI) catalyzed by ZnO nanoparticles, J. Hazard. Mater., 187 (2011) 258–263.
[36] W. Ketir, G. Rekhila, M. Trari, A. Amrane, Preparation, characterization and application of CuCrO2/ZnO photocatalysts for the reduction of Cr (VI), J. Environ. Sci., 24 (2012) 2173–2179.
[37] S. Sadeghi, M. Haghighi, P. Estifaee, Methanol to clean gasoline over nanostructured CuO–ZnO/HZSM-5 catalyst: influence of conventional and ultrasound assisted co-impregnation synthesis on catalytic properties and performance, J. Nat. Gas Sci. Eng., 24 (2015) 302–310.
[38] J. Lu, D. Schryvers, M. Roeffaers, E. Bartholomeeusen, B. Sels, Microstructure and intergrowth of defects in coffin-shaped ZSM-5 zeolite crystals revealed by FIB-assisted HRTEM.
[39] G.B.F. Seijger, O.L. Oudshoorn, W.E.J. van Kooten, J.C. Jansen, H. van Bekkum, C.M. van den Bleek, H.P.A. Calis, In situ synthesis of binderless ZSM-5 zeolitic coatings on ceramic foam supports, Microporous Mesoporous Mater., 39 (2000) 195–204.
[40] G. Flores, J. Carrillo, J. Luna, R. Martínez, A. Sierra-Fernandez, O. Milosevic, M.E. Rabanal, Synthesis, characterization and photocatalytic properties of nanostructured ZnO particles obtained by low temperature air-assisted-USP, Adv. Powder Technol., 25 (2014) 1435–1441.
[41] F. Yaripour, Z. Shariatinia, S. Sahebdelfar, A. Irandoukht, Conventional hydrothermal synthesis of nanostructured H-ZSM-5 catalysts using various templates for light olefins production from methanol, J. Nat. Gas Sci. Eng., 22 (2015) 260–269.
[42] F. Rahmani, M. Haghighi, Y. Vafaeian, P. Estifaee, Hydrogen production via CO2 reforming of methane over ZrO2-Doped Ni/ZSM-5 nanostructured catalyst prepared by ultrasound assisted sequential impregnation method, J. Power Sources., 272 (2014) 816–827.
[43] S. Aghamohammadi, M. Haghighi, S. Karimipour, A comparative synthesis and physicochemical characterizations of Ni/Al2O3–MgO nanocatalyst via sequential impregnation and sol–gel methods used for CO_2 reforming of methane, J. Nanosci. Nanotechnol., 13 (2013) 4872–4882.
[44] R. Khoshbin, M. Haghighi, Direct syngas to DME as a clean fuel: the beneficial use of ultrasound for the preparation of CuO–ZnO–Al2O3/HZSM-5 nanocatalyst, Chem. Eng. Res. Des., 91 (2013) 1111–1122.
[45] N. Mohaghegh, M. Tasviri, E. Rahimi, M.R. Gholami, Nano sized ZnO composites: preparation, characterization and application as photocatalysts for degradation of AB92 azo dye, Mater. Sci. Semicond. Process., 21 (2014) 167–179.
[46] O. Korkuna, R. Leboda, J. Skubiszewska-Zie¸ba, T. Vrublevs'ka, V.M. Gun'ko, J. Ryczkowski, Structural and physicochemical properties of natural zeolites: clinoptilolite and mordenite, Microporous and Mesoporous Mater., 87 (2006) 243–254.
[47] M. Khatamian, B. Divband, A. Jodaei, Degradation of 4-nitrophenol (4-NP) using ZnO nanoparticles supported on zeolites and modeling of experimental results by artificial neural networks, Mater. Chem. Phys., 134 (2012) 31–37.
[48] D.W. Breck, *Zeolite molecular sieves*, Krieger, Malabar, FL (1984).
[49] M.A. Behnajady, N. Mansoriieh, N. Modirshahla, M. Shokri, Influence of operational parameters and kinetics analysis on the photocatalytic reduction of Cr (VI) by immobilized ZnO, Environ. Technol., 33 (2012) 265–271.
[50] D.P. Das, K. Parida, B.R. De, Photocatalytic reduction of hexavalent chromium in aqueous solution over titania pillared zirconium phosphate and titanium phosphate under solar radiation, J. Mol. Catal. A: Chem., 245 (2006) 217–224.
[51] S. Liu, Removal of copper (VI) from aqueous solution by Ag/TiO2 photocatalysis, Bull. Environ. Contam. Toxicol., 74 (2005) 706–714.
[52] T. Liu, Z.-L. Wang, X. Yan, B. Zhang, Removal of mercury (II) and chromium (VI) from wastewater using a new and effective composite: pumice-supported nanoscale zero-valent iron, Chem. Eng. J., 245 (2014) 34–40.
[53] M.A. Behnajady, S. Bimeghdar, Synthesis of mesoporous NiO nanoparticles and their application in the adsorption of Cr (VI), Chem. Eng. J., 239 (2014) 105–113.
[54] Y. Ku, I.-L. Jung, Photocatalytic reduction of Cr (VI) in aqueous solutions by UV irradiation with the presence of titanium dioxide, Water Res., 35 (2001) 135–142.
[55] Q. Wu, J. Zhao, G. Qin, C. Wang, X. Tong, S. Xue, Photocatalytic reduction of Cr (VI) with TiO2 film under visible light, Appl. Catal. B, 142 (2013) 142–148.
[56] Q. Sun, H. Li, S. Zheng, Z. Sun, Characterizations of nano-TiO2/diatomite composites and their photocatalytic reduction of aqueous Cr (VI), Appl. Surf. Sci., 311 (2014) 369–376.
[57] H.-T. Hsu, S.-S. Chen, Y.-F. Tang, H.-C. Hsi, Enhanced photocatalytic activity of chromium (VI) reduction and EDTA oxidization by photoelectrocatalysis combining cationic exchange membrane processes, J. Hazard. Mater., 248 (2013) 97–106.
[58] A. Idris, N. Hassan, N.S.M. Ismail, E. Misran, N.M. Yusof, A.-F. Ngomsik, A. Bee, Photocatalytic magnetic separable beads for chromium (VI) reduction, Water Res., 44 (2010) 1683–1688.
[59] Q. Wang, J. Hui, L. Yang, H. Huang, Y. Cai, S. Yin, Y. Ding, Enhanced photocatalytic performance of Bi2O3/H-ZSM-5 composite for rhodamine B degradation under UV light irradiation, Appl. Surf. Sci., 289 (2014) 224–229.
[60] X. Huang, J. Yuan, J. Shi, W. Shangguan, Ozone-assisted photocatalytic oxidation of gaseous acetaldehyde on TiO2/H-ZSM-5 catalysts, J. Hazard. Mater., 171 (2009) 827–832.

[61] X. Liu, L. Pan, Q. Zhao, T. Lv, G. Zhu, T. Chen, T. Lu, et al., UV-assisted photocatalytic synthesis of ZnO–reduced graphene oxide composites with enhanced photocatalytic activity in reduction of Cr (VI), Chem. Eng. J., 183 (2012) 238–243.
[62] M.H. Farzana, S. Meenakshi, Photocatalytic aptitude of titanium dioxide impregnated chitosan beads for the reduction of Cr (VI), Int. J. Biol. Macromol., 72 (2015) 1265–1271.
[63] R.C. Pawar, C.S. Lee, Sensitization of CdS nanoparticles onto reduced graphene oxide (RGO) fabricated by chemical bath deposition method for effective removal of Cr (VI), Mater. Chem. Phys., 141 (2013) 686–693.
[64] M. Shirzad-Siboni, M. Farrokhi, R. Darvishi Cheshmeh Soltani, A. Khataee, S. Tajassosi, Photocatalytic reduction of hexavalent chromium over ZnO nanorods immobilized on kaolin, Ind. Eng. Chem. Res., 53 (2014) 1079–1087.
[65] S. Wei, Y. Chen, Y. Ma, Z. Shao, Fabrication of CuO/ZnO composite films with cathodic co-electrodeposition and their photocatalytic performance, J. Mol. Catal. A: Chem., 331 (2010) 112–116.
[66] M. Shirzad Siboni, M. Samadi, J. Yang, S. Lee, Photocatalytic reduction of Cr (VI) and Ni (II) in aqueous solution by synthesized nanoparticle ZnO under ultraviolet light irradiation: a kinetic study, Environ. Technol., 32 (2011) 1573–1579.
[67] A.R. Esfahani, S. Hojati, A. Azimi, M. Farzadian, A. Khataee, Enhanced hexavalent chromium removal from aqueous solution using a sepiolite-stabilized zero-valent iron nanocomposite: Impact of operational parameters and artificial neural network modeling, J. Taiwan Inst. Chem. Eng., 49 (2015) 172–182.